An Inquiry into the Effect of Freezing Methods on the Performance of a Crosslinked Alginate Membrane

A Major Qualifying Project
Submitted to the Faculty of
Worcester Polytechnic Institute
In partial fulfilment of the requirements
For the degree in Bachelor's of Science
In
Chemical Engineering

By

Reshawn George
Timothy Kendall
H La Vallee
Karla Navarro

Date: April 28, 2022
Project Advisor: Professor Andrew Teixeira (CHE)

Acknowledgements

This paper and the research would not have been possible without the help we received from others. First and foremost, we would like to thank our sponsor Incredible Foods for their generous contributions and assistance from Dr. Chris Hango and Dr. Marty Kolewe. We are immensely grateful for the guidance from Prof. Andrew Teixeira, our project advisor. We would also like to show gratitude to the following people who have contributed their time and expertise to help us accomplish this project:

- Dr. Geoffrey Tompsett for his time and assisting us with Raman Spectroscopy
- Prof. Christopher Brown and Connor Cumming for their expertise in the Surface Metrology Lab
- Doug White and Ian Anderson for their help around Goddard Hall and in determining appropriate methods to use
- Jyotsna Patel for her time and assistance with microtomy
- Doug Leonardi and Prof. Nancy Burnham for their time in the User-Friendly Characterization Lab
- Ruben Bonilla-Santiago for his guidance accessing analytical equipment
- Andy Butler for his time and assistance in obtaining NMR spectra for our samples

Abstract

Freezing food products is a valuable step in bringing them to market; as it has benefits in the ease of shipping, distribution, and the quality of the product when it makes it to shelves. Incredible Foods has created a line of products that utilize crosslinked sodium alginate (SA)-based hydrogel membranes to encapsulate various core food products. The impacts of deformation caused by freezing or dehydrating on the performance of crosslinked SA membranes, as well as the relative performance of membranes composed of two alternate SA sources are reported. The extent of deformation was quantified by using optical profilometry to measure membrane surface roughness, and image processing to determine the prevalence and size of surface defects. The impact on performance was quantified with steady-state permanence, calculated from a change in humidity of a passing air stream using a test cell. All freezing types tested besides flash freezing in dry ice demonstrated an increase in surface roughness, conventional freezing increased roughness and defect prevalence the most in all deformation methods tested. Dehydration caused a decrease in surface roughness with no significant change in defect prevalence. Permeance was not significantly affected by any deformation applied, suggesting the mechanism for water transport is not impacted by surface defects caused by freezing or dehydration. Membranes composed of high-viscosity SA were significantly smoother but slightly more permeable versus control. Understanding the impact of common deformations on the quality and performance of the SA hydrogel will lead to more insight into an effective manufacturing and shipping procedure, and comparing alternate alginate sources can further assist Incredible Foods in creating high quality, healthy and convenient food products.

Table of Contents

List of Tables

List of Figures

Authorship

Section	Author(s)	Editor(s)
Abstract	HL	KN
1. Introduction	KN	HL
2. Technical Background	-	-
2.1 Edible Films	RG	KN
2.2 Biopolymer Hydrogels	TK	RG
2.3 Alginate Hydrogel Membranes	HL	TK
2.4 Analytical Techniques	-	-
2.5 Surface Metrology	TK	HL
2.5 Freezing as a Form of Deformation	RG	KN
2.6 Water Transport Mechanisms	RG	TK
3. Methodology	KN	HL
3.1 Membrane Preparation	KN	HL
3.2 Constructing a Cell for Steady-State Permeance Testing	KN	TK
3.3 Surface Metrology	HL/KN	RG
3.4 Applying Deformations to Samples	TK/KN	HL
4. Results	-	-
4.1 Profilometric Properties	-	-
4.1.1 Optical Imaging	KN	TK
4.1.2 Surface Defect Size and Distribution	KN	RG
4.1.3 Surface Roughness	HL	KN
4.2 Steady-State Permeance	TK	KN
5. Discussion	-	-
5.1 Surface Metrology	HL	TK
5.2 Surface Defect Analysis	KN	HL

5.3 The Effect of Deformation on Permeance	TK	KN
5.4 Error and Variability of Membranes	RG	KN
6. Conclusions	RG	KN
7. Recommendations	HL	TK
Appendices	-	-
Appendix A. Variable Air Flow Rate	TK	All
Appendix B.1 Surface Defects Table	KN	All
Appendix B.2 Surface Metrology	HL	All
Appendix C. Permeance Cell Sample Calculations	KN	All
Appendix D. Permeance Cell Data Tables	KN	All

1. Introduction

Since the 1930s, freezing has been an essential part of the food manufacturing and distribution process.[1] Freezing food allows for preservation for extended periods of time and prevents the growth of microorganisms that could lead to food spoilage and illness.[2] When food is frozen at peak quality and kept frozen, it is said to retain vitamin content, texture, color, and flavor.[2] The food industry is still changing and improving the methods by which food is frozen to preserve the quality and safety of products; but how much does freezing really affect the food?

The team's sponsor, Incredible Foods, aims to make food more nutritious, accessible, and enjoyable for all.[3] Their technology platform can be used to directly address key sustainable development targets, by creating nutrient-dense food forms that last longer, utilize diverse ingredient inputs, and reduce packaging waste. Incredible Foods uses plant-based, vegan, gluten-free, and non-GMO ingredients.[3] They strive to provide nutritious food by never using artificial colors, flavors, preservatives, or sweeteners. Incredible Foods aims to make food accessible by making nutritious snacks more portable. Additionally, they are introducing new textures and taste interactions with their FoodBerry™ products; fruit barrier technology allows for the creation of berries from almost any food item imaginable. A FoodBerry™ mimics the structure and function of botanical fruit with a protective coating surrounding a more delicate, nutritious, and delicious core.[3] Most recently, Incredible Foods released plant-based ice cream treats. These treats not only had to stay frozen during manufacturing but also during shipping. To ensure that the Sundae & Smoothie Boms reached the consumer in a frozen state, the packages were sent with dry ice.

The project team has been asked to provide Incredible Foods with insight into how manufacturing processes could be affecting the physical characteristics of the membrane. This inquiry will bring to light correlations between the surface metrology of the membrane and the permeance of water through the membrane. More specifically, the team will study the effects of different deformations on the water transport properties of a sodium alginate hydrogel membrane. In the following chapters, the project team will review literature that has been done in this field, outline our research, review our results, and finally make recommendations.

2. Technical Background

2.1 Edible Films

Companies such as Incredible Foods have found ways to utilize food membranes to serve as a skin around the food, which works as a protective shell and also compliments the texture and flavor of the food product. For example, one of Incredible Foods' products is a ball of hummus that has an outer layer that tastes like roasted red bell pepper.[3] The outer pepper layer serves as both the packaging and as part of the eating experience. Edible films can also help extend the shelf life of a food product by "selectively allowing for controlled exchange of important gases such as oxygen and carbon dioxide".[4] They have a host of other benefits such as being great methods for inserting additives and for using excess food production.[5]

However, there are tradeoffs with edible membranes; lipid-based membranes generally have poor physical strength due to being quite brittle but have great water retention capabilities thanks to their nonpolar nature. While protein and polysaccharide-based membranes do not retain water as effectively due to their polar nature yet have better physical and sensory properties. Oftentimes in order to create food barriers that are both physically stable enough for transport and that have low water permissibility, lipids are added to polysaccharide membranes.[444] In this paper, the properties of alginate-based membranes are explored. Sodium Alginate is already used in food storage with a combination of sodium alginate and glycerol being used in coatings on fruits to help "contribut[e] to the delay of degenerative processes, maintaining color, polyphenols and anthocyanins, and improving overall fruit quality after harvest".[6] Sodium alginate barriers have great strength and have no flavor, making them a perfect base barrier.

2.2 Biopolymer Hydrogels

Hydrogels are gels that contain water trapped by a surrounding three-dimensional network. This network is composed of crosslinked proteins and/or polysaccharides, creating a polymer having properties that differ greatly depending on the monomer composition.[7] A significant body of literature exists focusing on distinct hydrogels with specific, targeted purposes, often concerning drug delivery, which can be compared to one another in order to observe similarities correlating to composition.[8]

Interest in the use of hydrogels in the food science field continues to grow as new applications for hydrogels as packaging for food or as carriers of active components emerge. Hydrogels represent a biodegradable alternative to plastic packaging, often resulting in lower environmental impact while still increasing shelf-life of degradable products.[9] When considered as packaging, they can take the form of membranes surrounding the food product, which can be characterized in terms of how effective they are at performing their duty: keeping food fresh and free of some damage. They regulate water loss and can provide antimicrobial activity.[10]

Hydrogels provide a means to integrate hydrophobic bioactive compounds into food and assist with and can be designed for the specialized release of these compounds into the body. Zhang et al. reviewed this type of design focused on the release of such compounds at various stages of the gastrointestinal tract, portraying the contributing hydrogel properties such as effective volume fraction, pore size, and cross-linking[11]. While these uses seem promising, the use of hydrogels is mainly concentrated in the biomedical industry and has yet to see widespread use in the areas of food and agriculture, as more research and effort is needed to optimize for widespread use.

2.3 Alginate Hydrogel Membranes

The main mechanism studied in our experimentation and analysis is the crosslinking of alginate (a salt of alginic acid) when exposed to a source of calcium ions. The resulting gel is edible and strong enough to encapsulate a liquid or semisolid core. Alginate gels are further strengthened using chitosan or other polymers which can form a complex with the alginate when introduced to the gel during crosslinking. This makes the resulting membrane more chemically and mechanically strong.[12] Crosslinked SA is commonly used in molecular gastronomy, where it is referred to as “spherification” when the outer surface of the membrane is exposed to the crosslinking agent, and reverse spherification when the crosslinking agent is contained within the core of the product (resulting in inside-out crosslinking progress and a more tightly crosslinked inner surface).[12] Spherification is most used when the core is semisolid, highly viscous, or otherwise incompatible with the crosslinking agent (due to taste or otherwise), and reverse spherification is most common with a fully liquid core.[12]

2.3.1 Alginate

Sodium alginate ($C_6H_9O_7Na$) (SA) is a polysaccharide isolated from the cell walls of brown algae.[13] It is widely used for its ability to form a viscous gel on contact with water, often sold as a

food emulsifier or thickener. It is composed of two different monomeric blocks: mannuronic acid (M) blocks and guluronic acid (G) blocks. The polymer consists of a chain of these two blocks, which can be in any order. At a pH of higher than 3.5, it can release its cation to become negatively charged and therefore receptive to crosslinking by a divalent cation such as Ca^{2+} (which is most commonly used in the food industry).[12] These ions will bond with G-G structures in the alginate chain, and irreversibly join two chains together. As this can only occur with G blocks, the ratio of M to G blocks greatly affects the properties of the crosslinked polymer.[12,13] As long as sufficient Ca^{2+} is available, crosslinking will occur very rapidly to form a tight elastic gel.

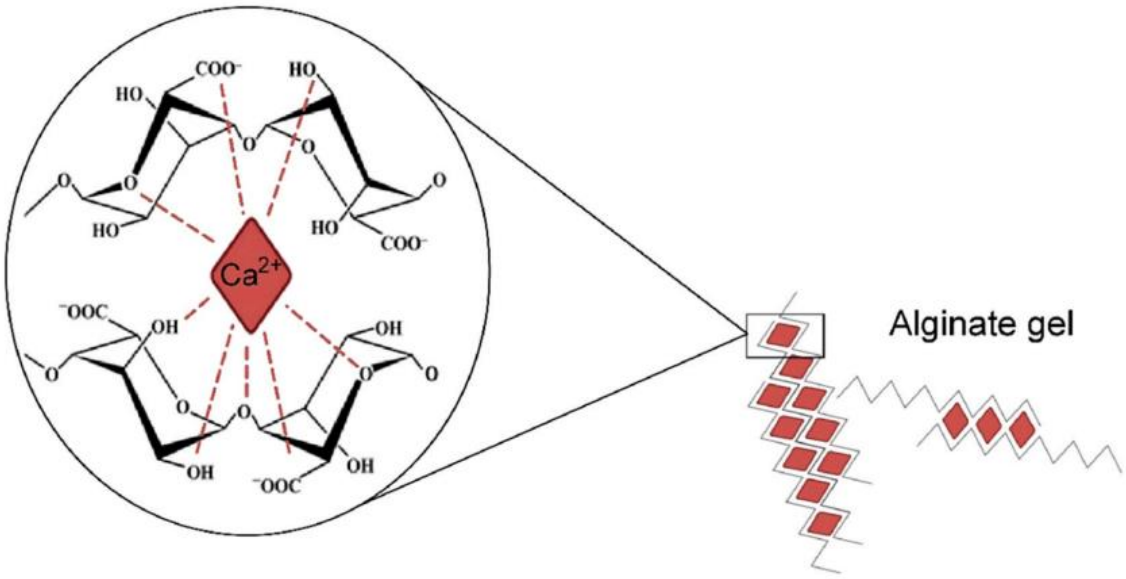

Figure 1: A model of the crosslinking mechanism between alginate G blocks and Ca^{2+} cations. Each positively charged calcium ion joins two G-G structures by an "egg-box" model, allowing the structure to become more complex and rigid. (Adapted from Martau et al., 2019)

2.3.2 Calcium

As the choice of calcium source does not significantly affect the crosslinking process, it is primarily determined based on other factors relevant to food safety and taste. Calcium chloride and calcium lactate are two of the most common calcium sources used in spherification and reverse spherification.[14] Calcium chloride is the simplest and most accessible, however, it imparts a bitter taste into the food when used for reverse spherification. Calcium lactate has a much less noticeable taste and is therefore chosen for use in our experiments and Incredible Foods' products.[14]

2.4 Surface Metrology

Surface metrology is the study of small changes in surfaces in order to provide insight as to how they interact with their environment and other surfaces. A number of modern techniques such as atomic force microscopy and mechanical (contact) and noncontact profilometry allow the user to characterize surfaces. Noncontact profilometry involves focused light to discern area topology by measuring light reflected off a surface as opposed to contacting methods, which drag a stylus across a surface to measure features and height differences.[15] This inquiry uses a Sensofar S neox optical profiler ("Sensofar"), which utilizes a focused LED tracing over a field of view and records the distance until the light hits the surface. This data is combined to form small-scale topographical maps and images as desired, as well as values representing the dataset, of which average roughness is a part. Several recent studies have been performed to assess surface features of organic polymers using the Sensofar. Xing et al.[16] determined the surface roughness of superhydrophobic polylactic acid membrane, and Shafqat and Hoefnagels[17] examined hydrogel fibers for surface damage while studying small-scale patterning.

2.5 Freezing as a Method for Deformation

Freezing is an important and common preservation process in the transportation and storage of many food products with high water content. Freezing inhibits microorganism growth and protein and fat degradation due to enzyme activity.[18] During the freezing process, the formation of ice crystals can impact the integrity of cells causing the quality of the products to lessen. The rate at which the freezing occurs "impacts the size and morphology of the ice crystals and their distribution inside the foods".[18] The formation of large, more damaging ice crystals is generally attributed to slower rates of freezing while high rates of freezing result in the better-preserved quality of the product. Large ice crystals can result in mechanical damage, denaturing of proteins, and discoloration of foods.[18] Zhang et al.[19] found that an increased freezing rate caused a smaller range of deformation, and that a smaller range of deformation corresponds to better preservation quality, when examining microscopic images of onion cells.

2.6 Water Transport Mechanisms

2.6.1 Diffusion in a Hydrogel

Diffusion is the net passive movement of molecules from areas of high concentration to areas of low concentration.[20] Diffusion through hydrogels is applied to a variety of applications such as drug delivery and membrane-based separation.[21] Diffusion in the hydrogel occurs due to a chemical potential difference between the water in the hydrogel and the water vapor or other source of water on the outside. When studying the ability of heydrogels to retain water to determine the impact of deformation, a characteristic value is desired to serve as a metric for performance. The general rate of water transfer through the membrane is referred to as the flux. However, flux is not a characteristic value and is dependent on factors such as volume and pressure.[22] Thus, it is more appropriate to use permeance when characterizing the membrane, as it is an inherent material property. The permeance of a material is a measure of its ability to diffuse water, independent of membrane thickness.[23]

2.6.2 Transport Through Pores

Pore-based water transport in cells is generally an active transport mechanism that relies on aquaporins or transport proteins. These proteins help the polar water molecule pass through the membrane.[24] However, in a hydrogel most water transport relies on slow diffusion through the membrane. This rate of diffusion can be increased by increasing the porosity or the size of pores in the hydrogel.[25] In this case the pores can further drive the rate of water transport through capillary action and forced convection.[26] This increase in porosity comes with disadvantages, with the increase in porosity coming at the cost of a decrease in mechanical properties such as Young's modulus and toughness. Such properties are important in food products that must withstand shipping and storing conditions which can often cause damage to the product.[27]

3. Methodology

To study the impact of freezing on the membranes of interest, the team completed a set of experiments using a set of performance metrics determined to be crucial in highlighting differences

between each membrane created. These metrics included water permeance, surface defect count/size, and surface roughness.

3.1 Membrane Preparation

A protocol was established to standardize membrane creation and create a standard sample for all tests. This was determined to be a 1 mm thick membrane produced in a 3D printed mold. Although a flat membrane sample is not as representative of Incredible Foods' products as a spherical mock product would be, it helped to isolate the properties of the material independent of the product size and internal composition.

Following a protocol provided by Incredible Foods, the crosslinked membrane was made from an alginate solution which was immersed in a crosslinking bath. The alginate solution was prepared from 2% SA in water heated to 90°C and then was cooled to 4°C before use. The proprietary crosslinking bath containing calcium lactate was prepared before the start of the experiment and stored at 4°C. One batch of crosslinking bath was reused for two months before it was replenished, as all reactants were in vast excess. Three distinct types of SA were used, and described in Table 1 below:

Table 1: A Summary of the types of sodium alginate used.

Acronym	Alginate
LV	The standard lower viscosity SA provided by Incredible Foods, produced by American International Chemical (AIC), with a reported viscosity of 35-45 mPas at 1%.
HV	A high-viscosity variant of SA-LV.
FC	An alternative source provided by FoodChem with a reported viscosity of 300-500 mPas at 1%.

The flat mold was 3D printed from PLA (Polylactic Acid) plastic in a flat capsule shape, 50mm wide, 25mm long, and 1mm deep. The SA solution was poured into this mold and scraped using a spatula to an even thickness of 1mm. The mold was then submerged in the crosslinking bath for 10 minutes to allow for complete interaction and crosslinking. After being removed from the crosslinking bath the membrane was washed gently with water before being used for analysis. See Figure 2 for an example of a completed sample.

Figure 2: A crosslinked sodium alginate membrane being lifted out of its 3D printed flat mold.

3.2 Constructing a Cell for Steady-State Permeance Testing

Water permeance was studied using a custom 3D printed device, seen in Figure 3 below. The permeance cell was sealed with Teflon tape and secured in place using electrical tape. Plumber's putty was used to seal any gaps between parts.

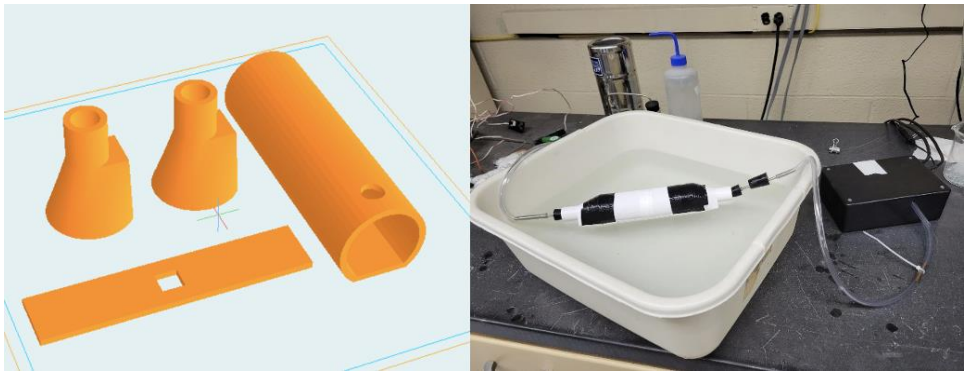

Figure 3: Water Permeance Test Apparatus. (left) CAD model of the permeability cell and (right) the assembled cell and test system including inline humidity sensor.

The membrane was secured to the bottom opening of the tube using the rectangular backing, to stay flush with the device, which was then placed in a water bath. As shown in Figure 4 below. The device allowed for constant air flow through the tube and constant contact with water on the bottom. A constant air flow was kept using compressed air, and the water level was kept constant as well. The flowrate of 1 L/min was verified by testing control membranes under different flows (Appendix A). Other equipment used consisted of a DAS relative humidity sensor

and a flow indicator used to regulate air flow. See Figure 4 for a schematic of the permeance test cell.

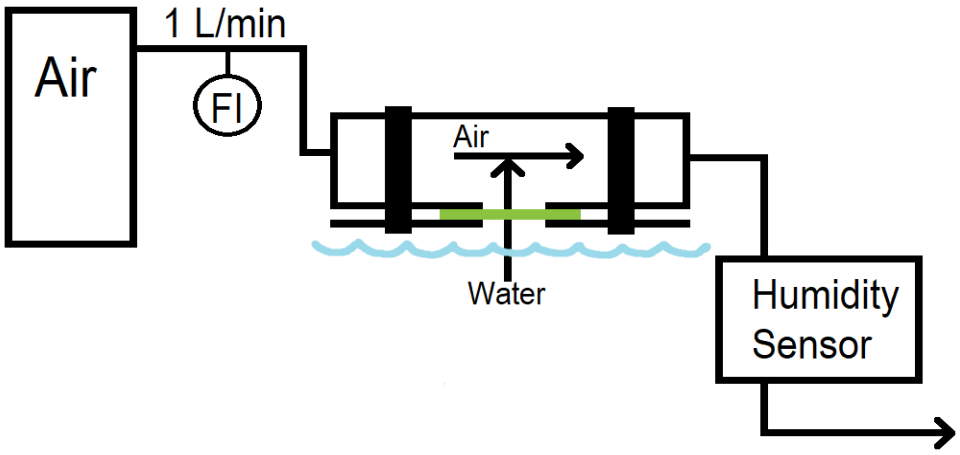

Figure 4: A schematic of the permeance cell built for the flat membrane (shown in green). The membrane is mounted in the cell and placed on the water's surface, with air flowing through the cell.

The purpose of this apparatus was to study the steady state permeance of water through the membrane. The humidity sensor provided information about the water content in the exiting air stream; this was converted to partial pressure using the ambient temperature and Antoine Equation. By comparing the humidity of the exiting air stream versus a baseline with no membrane, the amount of water that diffused through the membrane was determined. The flow rate of the water and air exiting the system was then found.

Due to the variability in temperature and humidity in the lab testing was conducted in, a calibration run was completed every day that testing took place. Calibration testing involved sealing the opening at the bottom of the cell with Teflon tape and securing with electrical tape; similar to the sample test set up, but without the sample and sample holder. The exiting water flow rate that resulted from these tests were subtracted from the air flow inlet of the sample tests run that day.

This allowed us to determine the steady-state flux of water, which was converted into permeance of the tested membrane using Equation 1. See Appendix C for full sample calculations.

$$\boldsymbol{Permeance} = \frac{\boldsymbol{J}}{\boldsymbol{\Delta C}} \qquad (1)$$

The flux was divided by the thermodynamic transmembrane driving force, the concentration gradient, to yield the permeance. This value is notably not a function of membrane thickness or the gas or liquid flowrates.

3.3 Surface Metrology

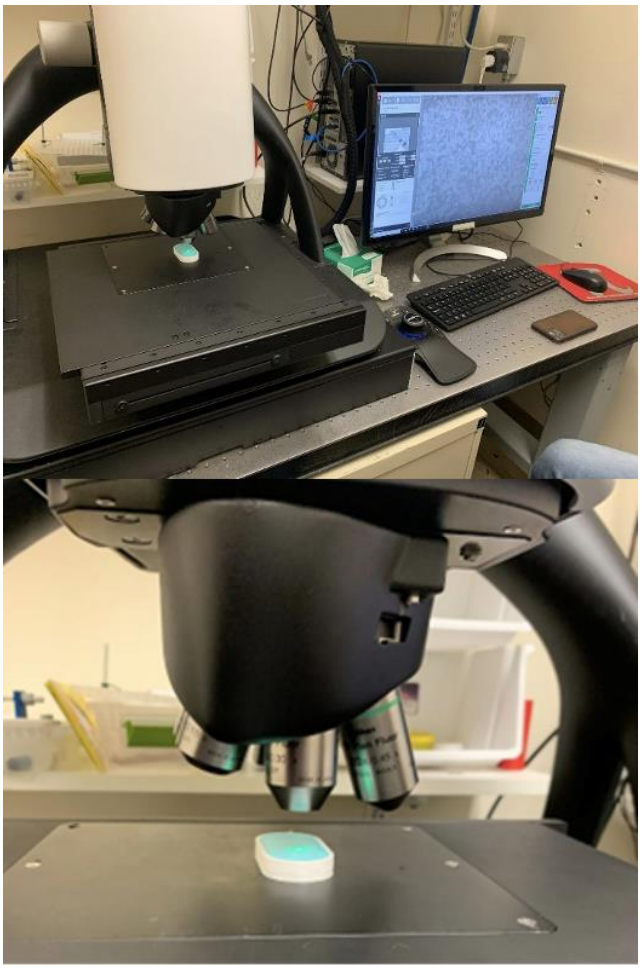

Figure 5: Sensofar S neox optical profiler with a loaded sample.

To further understand the ability of water to permeate through the membrane, the surface of the membrane was studied. A Sensofar S neox optical profiler and microscope ("Sensofar") was used to determine the average roughness of the samples (see Figure 5). High resolution images allowed for pore size distribution analysis. The sample was left in the mold and placed under the microscope. The microscope was set to 5x magnification, and a stitch scan was set to image the length of the membrane. Then, the software suite Mountains Lab by Digital Surf was used to conduct analysis on the profile data. For each sample analyzed, a 2-dimensional profile was

extracted from the topography. A polynomial curve was subtracted from this profile to remove large-scale curvature, and any aberrant end behavior was cropped. Finally, a roughness analysis was performed on the resulting profile, with an s-filter of 2.5 μm and an L-filter of 0.5 mm. This analysis resulted in a surface roughness (R_a) value along with other surface parameters.

ImageJ was used to analyze the pore size and distribution through manual measurements. Images obtained from the Sensofar were converted to 8-bit images. Then, the line tool was used to measure 1 mm on the scale bar in the image to set a scale in ImageJ. The oval select tool was used to manually select pores and the measure function was used to obtain the average area of the selected region. The individual measurements were then compiled in a list on ImageJ, which was then exported to an Excel sheet where the average area of the pores in the sample was obtained. Every sample underwent the same process to obtain the number of pores and the average pore size. Some images were a bit unclear, so contrast and brightness settings were manipulated to accentuate the pores in the sample images.

3.4 Applying Deformations to Samples

When a membrane is deformed, it is expected to perform poorly as compared to a non-deformed membrane. By deforming the membrane to varying degrees, it can be determined what degree leaves permanent impacts on performance. In order to simulate manufacturing, shipping, and food preparation conditions, membranes were subject to a variety of deformation conditions and compared to a standard undeformed sample. These conditions include freezing and thawing at three different speeds via three different freezing methods, as well as desiccation. Before tests were conducted, all samples were allowed to return to room temperature and were rehydrated by applying small amounts of water with a pipette to the surface of the membrane.

Conventional freezing was accomplished by membranes still in mold, placed in a sealed container in a freezer at -18°C until frozen (for at least 8 hours). Dry ice freezing was conducted in an ethanol-dry ice bath at -77°C. The mold containing the sample was placed in a pre-chilled container and then submerged in the bath for 5 minutes. For consistency, the container was also pre-chilled for 5 minutes in the dry ice-ethanol bath. Flash freezing using liquid nitrogen (-195°C), common to food manufacturing processes, was also tested. This was done by dipping the membrane in the mold, into a container holding liquid nitrogen; the membrane was submerged for 10 seconds.

Additionally, multiple freeze-thaw cycles illustrate potential less-than-ideal shipping conditions, where a product might either intentionally or unintentionally thaw out before consumption. In between each freezing type in the cycles, the membrane is allowed to come back to room temperature. Finally, desiccation was tested to determine the extent to which the membrane (and a potential product by extension) would be able to withstand being dried out and rehydrated. The membrane in its mold was allowed to dry at room temperature for at least 24 hours prior to testing. See Table 2 for a summary of all deformation types and freezing cycles tested.

Table 2: A Summary of Deformations Tested. See section 3.4 for full methodology for each deformation type.

Acronym	Deformation(s) Applied
CF	Conventionally frozen and thawed
DI	Frozen in dry ice-ethanol bath and thawed
LN2	Frozen in liquid nitrogen and thawed
DI-CF	DI followed by CF
LN2-DI	LN2 followed by DI
LN2-CF	LN2 followed by CF
LN2-DI-CF	LN2 followed by DI followed by CF
DH	Dehydrated and rehydrated fully

4. Results

In the following chapter, all major findings will be presented. Other results can be found in appendices as noted below.

4.1 Profilometric Properties

4.1.1 Optical Imaging

Images obtained from the Sensofar S neox optical profiler are included below. A micrograph of each sample preparation method is used to pinpoint key differences in each method. Each micrograph is representative of the entire surface scanned and the defects found on

the membrane surface. With each figure, a brief description of the surface defects found on the membrane is provided. A 1 mm scale bar is provided to aid in comparing surface defect sizes and distribution. In the following sections, the total amount of surface defects and defect size across the entire scan is compared.

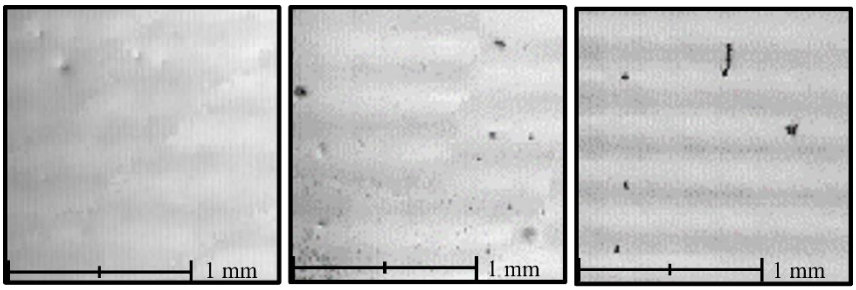

Figure 6: Micrographs of representative regions of undeformed samples: (a) undeformed low viscosity SA (b) undeformed high viscosity SA (c) undeformed SA from FoodChem. Minimal surface defects can be seen in an overall smooth surface.

Figure 6 above includes characteristic micrographs from each undeformed sample type. The surface of all three membranes appears to be flat and relatively free of defects. A few defects can be seen in the top left corner of the LV sample. The HV sample has a few more imperfections on the surface; there are circular defects as well as other areas of discoloration. The bottom left corner of the image shows a darker speckled region that was determined to not represent a surface defect by the standards of this inquiry. The most noticeable surface defects can be seen along the left side and in the bottom right corner. There are also a couple of small defects that can be seen along the top right side. The surface defects on the FC sample do not have quite as much depth to them, but they are very clear. There is also a long dark imperfection in the membrane in the top center of the image; this does not fit the criteria of a surface defect for this inquiry. This imperfection is more likely a fiber or dust particle that landed on the surface of the membrane during creation or before profilometry was conducted; therefore, it was omitted from the total defect count and size analysis. There are horizontal lines that appear across the entirety of the image, which is from the microscope beam and are likely to be a result of the transparent nature of the sample and do not indicate a deformation. These horizontal stripes are common among many scans and do not affect the roughness analysis.

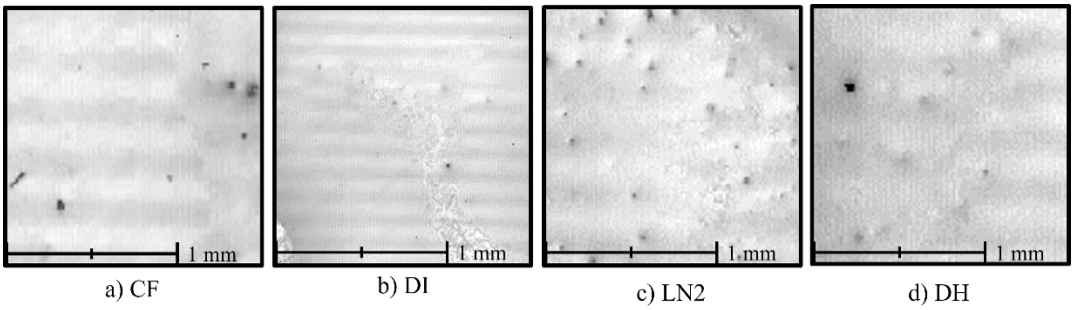

Figure 7: Micrographs of samples that underwent one form of deformation: (a) conventional freezing (b) dry ice – ethanol bath (c) dipped in LN2 (d) dehydrated and rehydrated. More deformations are present, with an apparent "bumpier" texture.

Figure 7 above represents the surface of the membrane samples that endured one form of deformation. In the CF sample, most defects can be seen along the right side; where there are a variety of defect sizes, from the smallest defect closest to the top left to the largest on the top-right edge. In the bottom left corner, there is one dark defect and one linear imperfection. The dark, linear imperfection by the left edge is most likely a fiber or dust particle on the membrane surface. All linear imperfections were omitted from the analysis done on surface defects. The defects found on the surface of the DI sample are very small and mostly found in the discolored region of the micrograph. On the other hand, there is a multitude of defects on the surface of the LN2 sample, which are very well defined. In the DH sample, there is really only one noticeable surface defect in the top left of the micrograph. Other defects can be seen in the diagonal region from the bottom left to the top right; these appear as small gray circles. The surface defects on the DH sample are not quite as defined as defects on other samples. Although not as defined, these defects appear to be larger than defects from previously shown samples. Once again, the horizontal stripes from the laser of the microscope are present in these images as well.

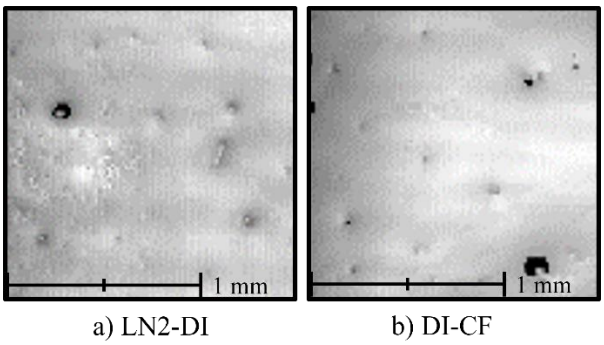

Figure 8: Micrographs representative of the entire samples that have undergone two forms of deformations: (a) LN2-DI and (b) DI-CF. Appear to be "bumpy" and surface defect are larger.

The figure above shows representative regions of samples that endured two sequential deformations. Both sample methods appear to have a similar number of defects on the surface, but the LN2-DI sample appears to have a bit more texture to it on the right side of the micrograph. The defects on both samples appear to be about the same size; both have larger defects than the aforementioned samples. The most noticeable defect on the LN2-DI sample can be found along the top left edge of the image. As for the DI-CF sample, the most noticeable defects are found in the bottom right corner of the image. In general, the DI-CF sample appears to have less texture to it, when compared to the LN2-DI sample. The horizontal stripes from the laser of the microscope are faintly present in these images as well.

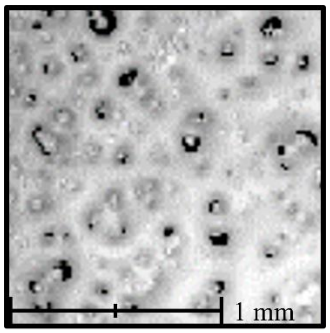

a) LN2-DI-CF

Figure 9: A Micrograph representative of the surface of a sample that underwent three forms of deformation: LN2-DI-CF. It is significantly more deformed, with more larger defects present.

Figure 9 shows the surface of a sample that underwent three forms of sequential deformation: the LN2-DI-CF sample. This sample has the most surface defects of all the sample types, as well as a variation in defect size. The image shows that there is no identifiable pattern to the defects, as the small and large defects are randomly scattered throughout the micrograph.

4.1.2 Defect Count and Size

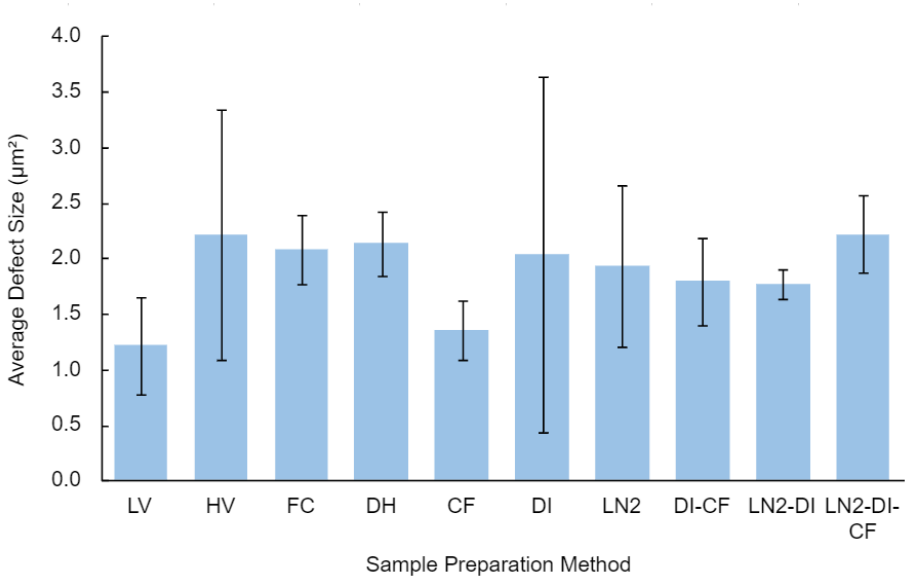

Figure 10: Average surface defect count of each sample preparation method. All deformed membranes have a larger number of surface defects versus the three undeformed controls (LV, HV, and FC).

As seen in Figure 10, almost all of the sample preparation methods had less than 600 defects on average, with the exception of the LN2-DI-CF method which averaged about 1,274 defects. The samples that were not deformed; SA-FC, SA-HV, and SA-LV had the lowest number of defects. However, there is a large error associated with each of these methods. The DH sample method also resulted in a low defect count. Of the different freezing methods, LN2-DI had the lowest defect count at 295 defects. The LN2 method averaged 272 defects but also had significant error. The DI method averaged 295 defects and had the smallest error of all the preparation methods. DI-CF and CF had similar defect counts around 350 defects.

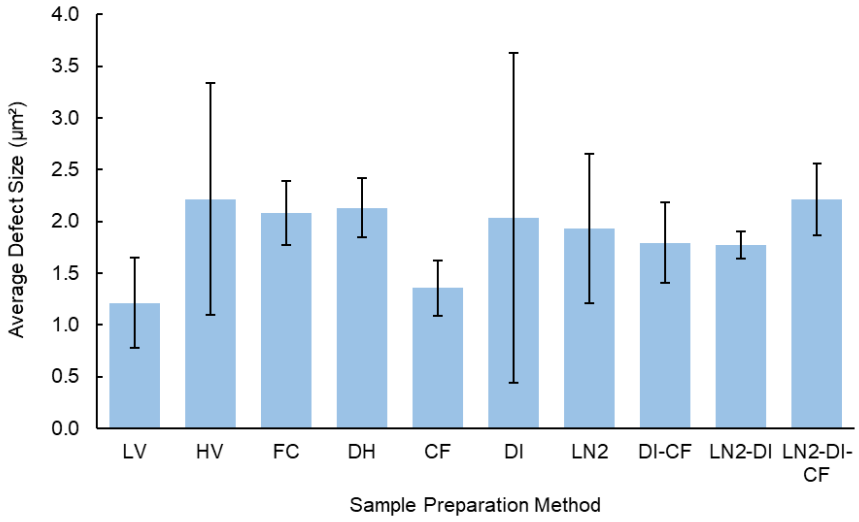

Figure 11: Defect size reported for each deformation type as an average of each trial imaged for that deformation type. Defect size was less conclusive than count, as all defects were in the same 1-2.5-micron range.

Figure 11 shows the average defect size for every sample preparation method. Defect size was determined by measuring the area of a defect. All defect sizes are of the same magnitude and relatively close in value. SA-LV and CF have the smallest average defect size, at 1.21 µm and 1.35 µm, respectively. LN2-DI-CF and SA-HV have the largest average defect size, at 2.22 µm and 2.21 µm, respectively. There are also large error bars on LN2, DI, and SA-HV.

4.1.3 Surface Roughness

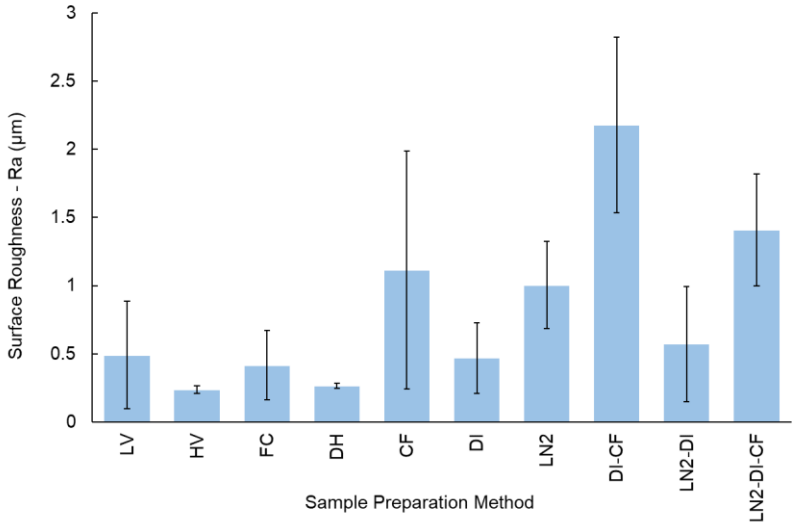

Figure 12: Average surface roughness results for each deformation type. Full profile data for each trial is given in Appendix B.

At least two trials were imaged for each deformation type, and a 3D topography was captured using confocal imaging with the Sensofar profiler. A representative strip from each sample was captured using a stitch of thirteen images traveling the length of the mold. Prior to imaging, the membranes were kept in a sealed container to prevent drying. After 3D imaging and analyzing the profile obtained from the topography, the mean average height (R_a, also known as average roughness) and calculated length were found as an average of all trials run for each deformation and different alginate source. Overall, the deformation that resulted in the roughest average surface was DI-CF (2.18 μm), and the deformation that was closest to the undeformed SA-LV was DI (0.47 μm vs. the control at 0.49 μm). DH was smoother than the control, at 0.27 μm. Most deformation types resulted in a higher R_a as compared to the control group, although several (DH, DI, and LN2-DI) were comparable or even slightly lower within error. Both alternate alginate sources had smoother profiles than the control when undeformed, although FC was very close to LV within error. Full reports including topography and profiles for each trial are in Appendix B.

4.2 Steady-State Permeance

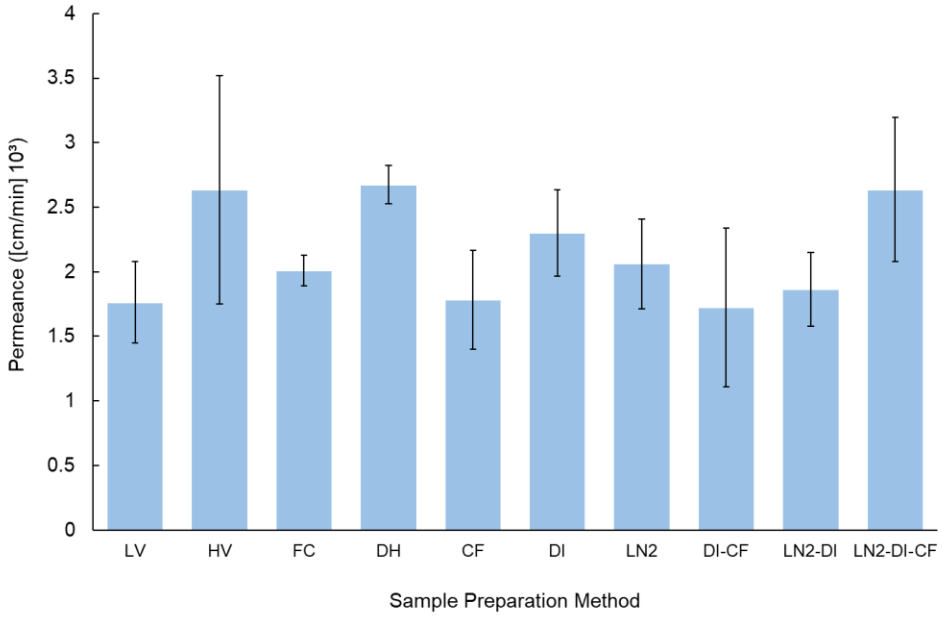

Figure 13: Average permeance results for each deformation type. Full permeance data can be found in Appendix D.

A minimum of four trials were performed for each type of deformation and alternate alginate sources, and the average permeance values of each group are compared in Figure 13. All results are compiled in Appendix D. Additionally, the flowrate of air into the cell was varied to validate the choice of 1L/min as a set airflow. These results are tabulated in Appendix A.

5. Discussion

5.1 Surface Metrology

When comparing roughness data acquired for each deformation type, the expected result would be that all deformed membranes have higher roughness than the control. However, in this study it is shown that some deformation types have a very small or even inverse effect on the roughness of the resulting membrane. The three deformed membranes that have comparable or even lower roughness than the control (SA-LV) are DI, DH, and LN2-DI.

DI represented a "flash" freezing situation, where the membrane is chilled quickly in a convective environment. This resulted in a slight increase in roughness due to the formation of ice crystals that expand to disrupt the crosslinked gel. However, as the freezing occurred quickly (less than 5 minutes in all trials), large ice crystals did not have a chance to form. This is because rapid freezing introduces a large number of nucleation sites for crystals to form, and this leads to many small ice crystals as opposed to fewer large ones that would expand and disrupt the surface of the membrane to a greater extent. This is validated by the negligible change in roughness (avg. 0.02 µm smoother) versus control

DH was not a freezing condition, and instead represented a product that has been left to dry (intentionally or unintentionally). It was not associated with an increase in roughness but was in fact calculated to be about 30% smoother than the undeformed control. This is likely due to the method used to freeze and then rehydrate the membrane. Each trial consisted of the membrane being left to dry for at least 8 hours after being crosslinked in its mold. During this time, the structure of the membrane collapsed as a result of its high (~98%) water content, becoming a fragile, thin film. Once water was reintroduced, the membrane was able to absorb it and reform. The optical imaging and topology studies show that the membrane is able to reform to a similar state to before it was dehydrated, assuming it is not disturbed during this time. Some more fragile

surface features may have been destroyed or not reformed completely during rehydration, leading to a smoother overall surface.

LN2 and CF consistently increased surface roughness when they were present in a freezing cycle and resulted in membranes that were about twice as rough on average versus the undeformed control. These freezing types both allowed for greater deformation of the membrane, but via two different mechanisms. LN2, while the fastest of all freezing types tested, was the only one to feature direct contact with a volatile substance (or the fast-moving, bubbling vapors produced by it). During the time spent submerged in liquid nitrogen, LN2-deformed membranes were being battered by turbulent bubbles and potentially splashes of the cold liquid. This resulted in larger deformation shown by an increase in roughness of 0.51µm as the surface was being impacted by these forces. CF was the warmest of the three freezing types, and therefore the freezing time was the longest. Conversely to DI as explained above, CF allowed for the formation of larger ice crystals as the freezing was slow enough for ice crystal nucleation sites to combine and expand more drastically, tearing small holes in the membrane in the process which resulted in a rougher surface, increasing roughness by 0.62µm once thawed.

5.2 Surface Defect Analysis

The data collected is indicative that surface defects are present after deformations are applied. The LN2-DI-CF sample preparation had six times more surface defects than the control (LV). Both single and sequential deformations were on average higher than the control; however, neither surpassed six hundred surface defects. When comparing deformation methods, it is important to consider the error associated with each of them. The LN2-DI-CF deformation method has the largest amount of surface defects, even when accounting for error.

The undeformed samples had noticeable surface defects; this shows that some defects are present prior to deformation. Therefore, the likelihood that all defects counted were in fact surface defects is low. It is possible that the defects are air bubbles trapped under or on the surface of the membrane during crosslinking or when the SA was poured into the mold. However, it has been shown that the freezing process creates more surface defects. The undeformed samples had a lower defect count on average compared to the freezing methods. On the other hand, the DH samples had only a 0.9% difference when compared to the control (LV). This leads to the conclusion that defects are created during the freezing process (see Figure 11).

The size of surface defects on the membrane is not significantly influenced by the deformation applied. On average, all surface defects (on all samples), were 1 to 2.5 μm^2 in area. Figure 12 shows that there is not a large variance of defect size that correlates to deformation methods. The control samples have the lowest defect size, on average, followed by the CF samples. This was unexpected, as the CF method promotes the growth of large ice crystals to form for an extended amount of time. Also unexpectedly, the other two undeformed methods (HV and FC) had a large average size of defects, comparable to the other freezing methods. Further analysis of SA composition would be required to determine the mechanism governing defect formation on membranes made from alternate undeformed SA sources.

Initially, it was hypothesized that these defects were pores, and therefore water transport would be correlated to defect size and/or count. However, as shown in Section 4.2, the permeance values are all relatively similar regardless of the freezing method. This shows that the surface defects are not a mechanism for transport and thus water flow is diffusion dependent. The diffusion coefficient for this transport should remain the same regardless of deformation, as the chemistry of the membrane does not change with freezing or dehydration.

5.3 The Effect of Deformation on Permeance

Water permeance was shown not to increase significantly from the control tests to deformed membranes. Permeance variability was generally high within each test group, indicated by higher standard deviation. This was especially true for testing involving dry ice, where exposure to the dry ice bath yielded the least consistent results.

Water loss from potential products appears to be influenced primarily from membrane composition as opposed to deformation. A higher-viscosity (HV) membrane was found to be 50% more permeable than its low-viscosity counterpart of the same source, which indicates that the larger the polymer's chain length, the more easily water can travel through a SA membrane. Further study might examine ultra-low or ultra-high viscosities in SA, to see if this trend holds.

Dehydrated membranes also performed similarly to fresh membranes, and it was observed that the material was able to contract and rehydrate with little difference to the membrane itself. The permeance cell used in this experiment was designed to be simple and effective, and required some design iteration mainly to keep the cell watertight. Effort was made to control small factors that affect permeance, but for best results trial groups should be run on the same day to

factor in the effect of the baseline run with no membrane, and the temperature of the water bath should be constant.

This experiment's results aid in the characterization of the physical nature of the hydrogel and indicate that these membranes represent resilient food technology. While it might prove unnecessary to reuse this type of membrane due to the simplicity of preparation, there could be applications for reusability, a factor that is relevant when considering this technology as a potential replacement for the widespread use of plastic packaging.

5.4 Error and Variability of Membranes

When looking at the relative error for each trial, LN2 had a large amount of variability compared to others when looking at the average amount of surface defects. This was likely due to the violent nature in which the membrane froze when it contacted LN2 of the volatile nitrogen vapor being released from it. The membranes would rapidly freeze and contract from the mold leading to cracking. This often caused the membranes to display more qualitative deformation and sometimes would even result in shattering.

There was also systematic error in some of the other methods. For example, in the dry ice trial the container the membranes sat in, when put into the ice bath, was pre chilled. This pre-chilling process was not completely controlled for as the temperature of the container was not recorded before the trial or between trials and instead it was just cooled for an approximate amount of time. This could make the initial temperature of the membranes differ and thus the cooling rate would not be consistent as the container would have spent longer in the ice in the later trials potentially giving a lower initial temperature. The team also encountered issues with the transient nature of the membrane as when running surface metrology, the membranes would begin to dry resulting in a rougher surface than expected. The team attempted to solve this by keeping the membranes in water, this could have also caused the surface roughness to not be reported correctly as the water could have interfered with the scan

There also appeared to be large variations in the membranes of the same trial. The team controlled the initial temperatures of both baths and used the same equipment for each batch production. Based upon the qualitative and quantitative differences between membranes of the same method, there were other unknown variables that were not being controlled for. The complete cycle trials resulted in a greater amount of error when looking at the average surface defect count

and the permeance value. This was because as there were more experiments run there were more variables to control. In general, there was high variability from batch to batch of membranes.

For future endeavors, producing all the membranes in one batch would help reduce error as then the environmental conditions of each membrane would be much more similar. For example, it was observed that on a particularly humid day, the relative humidity was globally higher. While single batches work well for frozen membranes, it is important to keep the membranes wet when not frozen to avoid unintentional deformation. Outside of this there will still be some unavoidable variability between membranes as they are all handmade. Due to time constraints associated with the nature of the project the team was unable to run as many trials as desired. This resulted in a large amount of potential error due to the variability associated with a small sample size. Future work should attempt to increase the number of trials to produce more conclusive data.

6. Conclusions

The project team was tasked with providing Incredible Foods insight into how manufacturing processes could be affecting the physical characteristics of the sodium alginate-based membrane that is used in some of their products. More specifically, the team studied the effects of different deformations on the water transport properties of a sodium alginate hydrogel membrane. It was observed that freezing SA membranes causes noticeable deformation, exhibiting higher average roughness values and increased number of surface defects. An exception to this, is when “flash” freezing in a dry ice bath, which caused minimal deformation due to the rapid speed of cooling and the convective environment, resulting in minimal opportunity for large ice crystal growth. Conversely, conventional freezing (which did allow for the formation of large ice crystals) or direct contact freezing with liquid nitrogen resulted in larger amounts of deformation as seen in the number of defects and average roughness values. However, it was found that deformations in the membranes do not significantly affect water transport properties, as shown by the permeance values. The difference in the permeance of each membrane was not statistically significant when accounting for error. These deformations did not affect water transport properties because the deformations seen on the membrane were not pores and were just caused by ice crystals during freezing, thus their increase did not increase permeance. The water transport through the membrane is diffusion driven, as opposed to pore driven which is common among non-hyper-

porous hydrogel membranes. This was demonstrated by the similar permeance values found for all trials regardless of preparation method.

The main conclusions are therefore as follows:

1. Freezing a sodium alginate membrane causes deformation, categorized by increased roughness and surface defects, which is more severe with conventional freezing or LN2 contact.
2. Flash freezing an SA membrane convectively at -77°C results in almost zero change to surface roughness. Dehydrating and rehydrating the membrane causes a decrease in surface roughness.
3. Deformations in the sodium alginate membrane's surface do not significantly impact water permeance.

7. Recommendations

Based on these findings, we recommend that Incredible Foods minimizes the temperature change of their products when possible and avoids multitype freezing processes on membranes for the sake of product mouthfeel. Conventional membrane freezing processes should be replaced with flash freezing as conventional freezing specifically caused surface roughness increase. Although it is difficult due to the variability in membrane production, Incredible Foods should investigate product uniformity.

If further study into this topic is pursued, the group has encountered additional areas of interest that may provide further insight into the overall product cycle, as well as other topics that may prove beneficial to Incredible Foods to research:

Further Testing using a Spherical Mock Product

The project team used a flat membrane mock product in this study, to isolate the SA membrane. However, a spherical mock product would be more representative of Incredible Foods' products as they consist of a frozen core of agar or a similar substance coated with a SA solution and dipped in a crosslinking bath. This could provide insight into how the surface of the spherical membrane compares to that of the flat membrane, since the spherical membrane thickness cannot be controlled. Additionally, performing similar deformation tests on spherical mock products could provide insight to unanticipated effects of the contents on the membrane itself, such as an

expansion of the core which could increase internal pressure, or impacts from ice crystals formed at the core-membrane interface.

Compare Freezing Cycles Without Intermediate Thawing

For each trial involving multiple freeze cycles, the membrane was fully thawed between deformations. It may be valuable to test multiple freezing types sequentially without thawing or with a partial thaw, to see if there is a way to transition between freezing types with minimal additional deformation. Additionally, testing multiple freeze cycles without thawing is likely more representative of the actual conditions of the product during manufacturing and shipping.

Physical Polymeric Properties

Determining the physical strength of the membrane through tensile testing would give another valuable metric of membrane performance. If a membrane is significantly weakened by a deformation process, it may burst or break when on a product (especially one with a liquid or semisolid core) or may have an adverse effect on mouthfeel or texture. Studying the effect of various deformations on the tensile strength of the membrane would paint a larger picture of the impact of deformation on performance.

Use NMR to gain insight into M and G Block Composition of Alginates

NMR analysis was planned from the beginning of this project but was unable to be fully completed. The team was able to acquire preliminary scans of the three different SA sources, which were sent to Incredible Foods for review. A full analysis would allow for a much better quantitative understanding of the differences between the three alginate sources tested, as it would allow for the assessment of the ratio of the two monomers (mannuronic acid and guluronic acid) which has been shown in literature to influence SA's performance when used as a membrane. This is a critical part of the full picture, and one that both the team and the sponsor would find to be incredibly valuable.

Bibliography

[1] Staff, E. The Strange History of Frozen Food https://www.eater.com/2014/8/21/6214423/the-strange-history-of-frozen-food-from-clarence-birdseye-to-the (accessed 2022 -04 -18).

[2] Freezing and Food Safety | Food Safety and Inspection Service http://www.fsis.usda.gov/food-safety/safe-food-handling-and-preparation/food-safety-basics/freezing-and-food-safety (accessed 2022 -04 -18).

[3] Homepage – Incredible Foods https://incrediblefoods.com/ (accessed 2021 -10 -26).

[4] Ansorena, M. R.; Pereda, M.; Marcovich, N. E. Edible Films. In Polymers for Food Applications; Gutiérrez, T. J., Ed.; Springer International Publishing: Cham, 2018; pp 5–24. https://doi.org/10.1007/978-3-319-94625-2_2.

[5] Hango, C. Incredible Foods, Boston, MA. Personal Communication, October, 2021.

[6] A Review of Edible Packaging for Foods https://www.ijcmas.com/abstractview.php?ID=13861&vol=8-7-2019&SNo=359 (accessed 2022 -04 -18).

[7] Bahram, M.; Mohseni, N.; Moghtader, M. An Introduction to Hydrogels and Some Recent Applications; IntechOpen, 2016. https://doi.org/10.5772/64301.

[8] Narayanaswamy, R.; Torchilin, V. P. Hydrogels and Their Applications in Targeted Drug Delivery. Molecules 2019, 24 (3), 603. https://doi.org/10.3390/molecules24030603.

[9] Shaikh, S.; Yaqoob, M.; Aggarwal, P. An Overview of Biodegradable Packaging in Food Industry. Current Research in Food Science 2021, 4, 503–520. https://doi.org/10.1016/j.crfs.2021.07.005.

[10] Shaikh, S.; Yaqoob, M.; Aggarwal, P. An Overview of Biodegradable Packaging in Food Industry. Current Research in Food Science 2021, 4, 503–520. https://doi.org/10.1016/j.crfs.2021.07.005.

[11] Zhang, Z.; Zhang, R.; Chen, L.; Tong, Q.; McClements, D. J. Designing Hydrogel Particles for Controlled or Targeted Release of Lipophilic Bioactive Agents in the Gastrointestinal Tract. European Polymer Journal 2015, 72, 698–716. https://doi.org/10.1016/j.eurpolymj.2015.01.013.

[12] Bennacef, C.; Desobry-Banon, S.; Probst, L.; Desobry, S. Advances on Alginate Use for Spherification to Encapsulate Biomolecules. Food Hydrocolloids 2021, 118, 106782. https://doi.org/10.1016/j.foodhyd.2021.106782.

[13] Lawrie, G.; Keen, I.; Drew, B.; Chandler-Temple, A.; Rintoul, L.; Fredericks, P.; Grøndahl, L. Interactions between Alginate and Chitosan Biopolymers Characterized Using FTIR and XPS. Biomacromolecules 2007, 8 (8), 2533–2541. https://doi.org/10.1021/bm070014y.

[14] Effect of calcium source and exposure-time on basic caviar spherification using sodium alginate - ScienceDirect https://www.sciencedirect.com/science/article/pii/S1878450X13000073?via%3Dihub (accessed 2022 -04 -18).

[15] DeRose, J.; Laforet, A. S.; Barbero, D. R. Brief Introduction to Surface Metrology. 2019.

[16] Xing, R.; Huang, R.; Qi, W.; Su, R.; He, Z. Three-Dimensionally Printed Bioinspired Superhydrophobic PLA Membrane for Oil-Water Separation. AIChE Journal 2018, 64 (10), 3700–3708. https://doi.org/10.1002/aic.16347.

[17] Shafqat, S.; Hoefnagels, J. P. M. Cool, Dry, Nano-Scale DIC Patterning of Delicate, Heterogeneous, Non-Planar Specimens by Micro-Mist Nebulization. Exp Mech 2021, 61 (6), 917–937. https://doi.org/10.1007/s11340-020-00686-2.

[18] Tan, M.; Mei, J.; Xie, J. The Formation and Control of Ice Crystal and Its Impact on the Quality of Frozen Aquatic Products: A Review. Crystals 2021, 11 (1), 68. https://doi.org/10.3390/cryst11010068.

[19] Zhang, X.; Chu, X.; Ji, H.; Wang, Y. Effect of Freezing Rate on the Onion Cell Deformation Evaluated by Digital Image Correlation. Food Anal. Methods 2016, 9 (11), 3125–3132. https://doi.org/10.1007/s12161-016-0504-8.

[20] Diffusion - Definition and Examples - Biology Online Dictionary https://www.biologyonline.com/dictionary/diffusion (accessed 2022 -04 -18).

[21] Fornasiero, F.; Tang, D.; Boushehri, A.; Prausnitz, J.; Radke, C. J. Water Diffusion through Hydrogel Membranes: A Novel Evaporation Cell Free of External Mass-Transfer Resistance. Journal of Membrane Science 2008, 320 (1), 423–430. https://doi.org/10.1016/j.memsci.2008.04.032.

[22] Soil Survey Technical Note 6 | NRCS Soils https://www.nrcs.usda.gov/wps/portal/nrcs/detail/soils/ref/?cid=nrcs142p2_053573 (accessed 2022 -04 -18).

[23] The Difference Between Permeance and Permeability https://www.buildingenclosureonline.com/blogs/14-the-be-blog/post/85873-the-difference-between-permeance-and-permeability (accessed 2022 -04 -18).

[24] Pohl, P. Chapter 9 - Water transport, H.T. Tien, A. Ottova-Leitmannova, Membrane Science and Technology, Elsevier, Volume 7, 2003, Pages 295-314, ISSN 0927-5193, ISBN 9780444509406, https://doi.org/10.1016/S0927-5193(03)80033-5. (https://www.sciencedirect.com/science/article/pii/S0927519303800335)

[25] Alsaid, Y.; Wu, S.; Wu, D.; Du, Y.; Shi, L.; Khodambashi, R.; Rico, R.; Hua, M.; Yan, Y.; Zhao, Y.; Aukes, D.; He, X. Tunable Sponge-Like Hierarchically Porous Hydrogels with Simultaneously Enhanced Diffusivity and Mechanical Properties. Advanced Materials 2021, 33 (20), 2008235. https://doi.org/10.1002/adma.202008235.

[26] Lee, S. J.; Kim, H.; Ahn, S. Water Transport in Porous Hydrogel Structures Analogous to Leaf Mesophyll Cells. Microfluid Nanofluid 2015, 18 (5), 775–784. https://doi.org/10.1007/s10404-014-1418-7.

[27] Alsaid, Y.; Wu, S.; Wu, D.; Du, Y.; Shi, L.; Khodambashi, R.; Rico, R.; Hua, M.; Yan, Y.; Zhao, Y.; Aukes, D.; He, X. Tunable Sponge-Like Hierarchically Porous Hydrogels with Simultaneously Enhanced Diffusivity and Mechanical Properties. Advanced Materials 2021, 33 (20), 2008235. https://doi.org/10.1002/adma.202008235.

Appendices

Appendix A. Variable Air Flow Rate

The flowrate of air into the cell was varied to validate the choice of 1 L/min (0.001m) as a set airflow. Steady state was achieved for all runs at a lower flowrate. The highest possible permeance, at 0.7 L/min, was not more desirable than 1 L/min, but represents a point where the airflow is able to transport the highest amount of water without the membrane drying at all due to the air. Figure 14 shows these trials, with the calculated permeance values against flowrate.

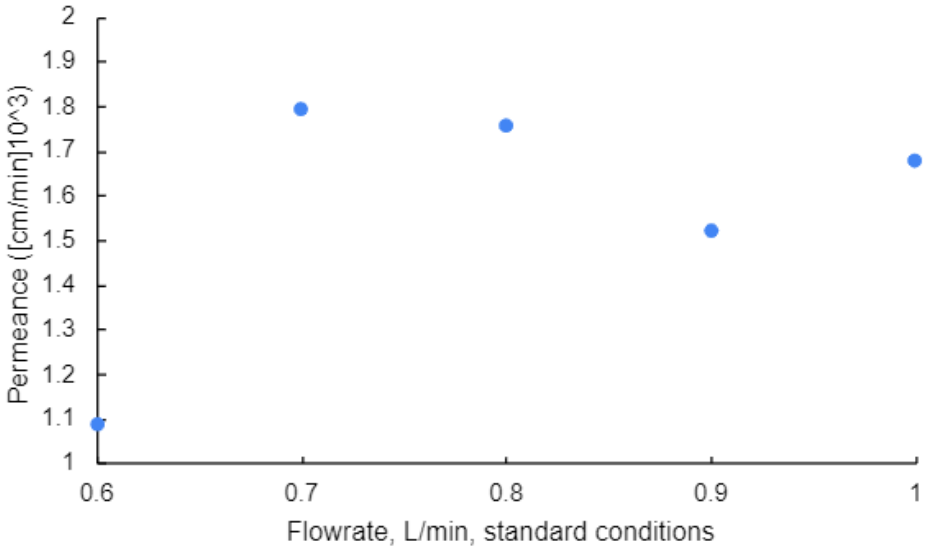

Figure 14: Permeance plotted against various air flow rates.

Appendix B. Roughness Data

Surface Defects Table

The table below contains the raw data of which was used to obtain the average values and standard deviation used in Results.

Table 3: Raw Data of Surface Defect Count for Every Sample Imaged.

Sample Type	Trial	Defect Count	Average Defect Area (μm²)	Trial	Defect Count	Average Defect Area (μm²)
LV	1	422	1.0229	2	120	1.0167
LV	3	60	0.9415	4	244	1.8642
HV	1	97	3.0106	2	287	1.4214
FC	1	259	2.303	2	93	1.8633
DH	1	252	1.9282	2	167	2.3336
CF	1	324	1.1677	2	365	1.5419
DI	1	300	3.1637	2	290	0.9079
LN2	1	78	2.4437	2	466	1.4188
DI-CF	1	441	2.0691	2	283	1.5166
LN2-DI	1	265	1.8594	2	213	1.6737
LN2-DI-CF	1	1835	2.4579	2	712	1.9669

Surface Metrology

Also included alongside this paper is a full report of surface topography and profile data collected from the methods described in Section 3 and summarized in Section 4.1.3. Reports were generated and composed using Mountains Lab 9. Data from each trial, including an image as well as a topographical map, is included, as well as 2-dimensional profiles extracted from each surface. All profiles have had a polynomial form removed to subtract any large-scale curvature, and some have been cropped to remove aberrant end behavior. Finally, a parameters table was created for each trial, including several parameters of the roughness profile including surface roughness (R_a).

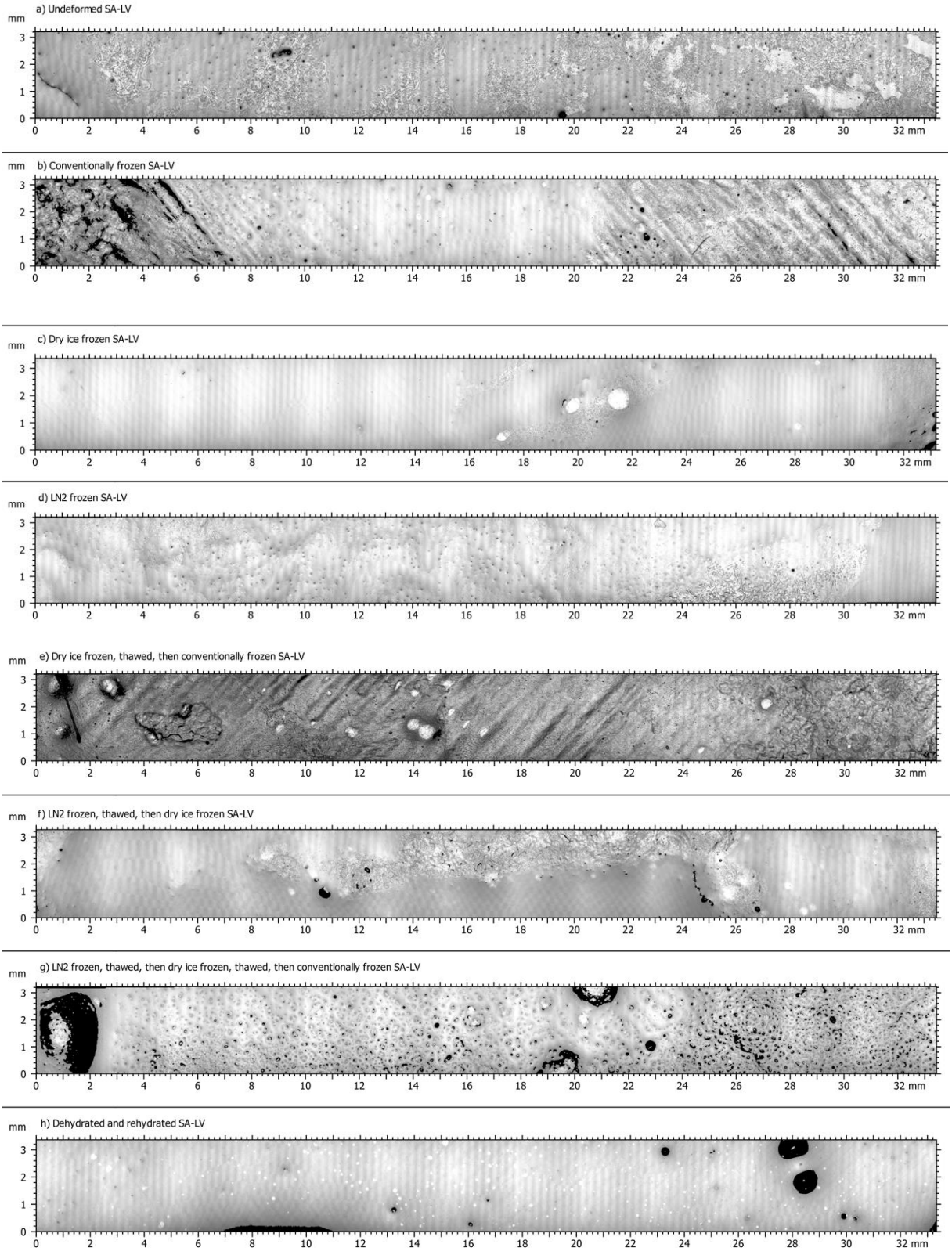
a) Undeformed SA-LV
b) Conventionally frozen SA-LV
c) Dry ice frozen SA-LV
d) LN2 frozen SA-LV
e) Dry ice frozen, thawed, then conventionally frozen SA-LV
f) LN2 frozen, thawed, then dry ice frozen SA-LV
g) LN2 frozen, thawed, then dry ice frozen, thawed, then conventionally frozen SA-LV
h) Dehydrated and rehydrated SA-LV
mm
0 1 2 3
0 2 4 6 8 10 12 14 16 18 20 22 24 26 28 30 32 mm

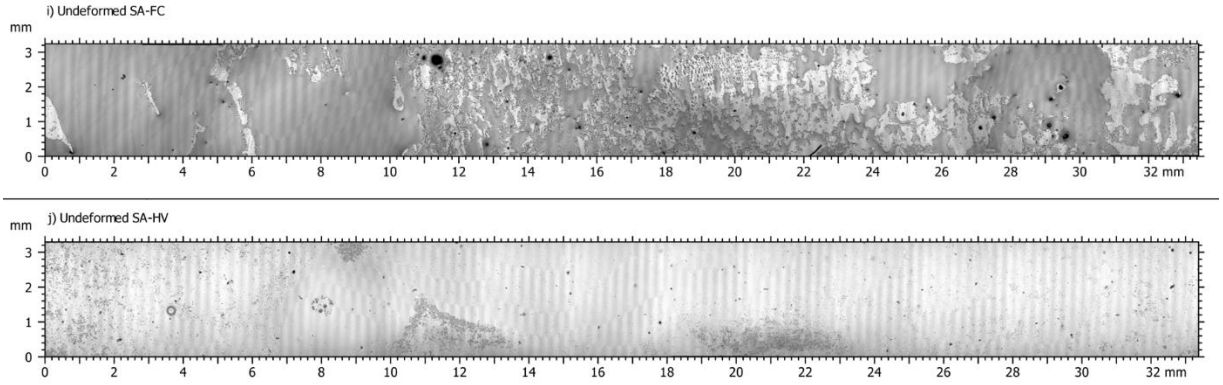

Figure 15: Full imaging data for each sample as analyzed with the Sensofar optical profiler, with scales and trial labels. Significant deformation can be observed on b), e), and g), while h), f), d), and c) appear fairly free of defects.

Appendix C. Permeance Cell Sample Calculations

The following sample calculation was conducted on the trial LV:1 and was used to convert relative humidity to permeance of water through the membrane for all other data acquired. Two main assumptions were made for these calculations:

Pressure (assumed to be standard): 101325 Pa

Inlet Air Flow: 1 L/min

From the humidity sensor in the experimental set up:

Relative Humidity %: 7.10

Temperature: 25.47 °C = 298.62 K

The Antoine Equation was used to correlate the temperature to the saturated vapor pressure, which was used to find the partial pressure of water in the exiting air stream.

$$log_{10}(p) = A - \frac{B}{C + T}$$

$p = Vapor\ Pressure\ (Pa)$

$T = Temperature\ (K)$

$A, B, C = Antoine\ coefficients$

Rearranged in terms of P:

$$p = 10^{A - \frac{B}{C+T}}$$

Under these conditions[1]:

A = 5.40221, B = 1838.675, C = -31.737

Therefore, the saturated vapor pressure is found to be:

$$p = 10^{(5.40221) - \frac{(1838.675)}{(-31.737)+(298.62\ K)}}$$

$$p = 32.5663\ bar = 3256\ Pa$$

The partial pressure of water is found by multiplying the saturated vapor pressure and the relative humidity:

$$P_{H2O} = p * \varphi = (3256.63\ Pa) * (0.0710) = 231.22\ Pa$$

The mole fraction of water is found by dividing the partial pressure of water by the total pressure:

$$x_{H2O} = \frac{P_{H2O}}{P_{total}} = \frac{231.22\ Pa}{101325\ Pa} = 0.00228$$

[1] Water. https://webbook.nist.gov/cgi/cbook.cgi?ID=C7732185&Mask=4&Type=ANTOINE&Plot=on (accessed 2022 -04 -18).

Next, the outlet flow of water is found by assuming that the total inlet gas flow is equal to the outlet gas flow. This assumption allows for the total outlet flow to be calculated using the known volumetric flow going into the system. From here, the mole fraction of water is used to find the outlet flow of water.

$$F_1 \cong F_2$$

$$F_1 = \left[\dot{V}\left(\frac{P}{RT}\right)\right]$$

$$F_{2,H2O} = x_{H2O} * F_2$$

$F_1 = Inlet\ Flow\ (L/min)$

$F_{2,H2O} = Outlet\ Flow\ of\ Water\ (L/min)$

$\dot{V} = Volumetric\ Flow\ Rate\ (sccm)$

$R = Ideal\ Gas\ Constant\ (^{m^3Pa}/_{K \cdot mol})$

Using standard conditions and an inlet flow rate of 1 L/min:

$\dot{V} = 1000\ sccm$ $P = 101325\ Pa$ $T = 298.62\ K$ $R = 8.314\ (\frac{m^3Pa}{K \cdot mol})$

Which gives:

$$F_1 = \left[\dot{V}\left(\frac{P}{RT}\right)\right] = \left[(0.001\ m^3/min)\left(\frac{101325\ Pa}{\left(8.314\frac{m^3Pa}{K \cdot mol}\right) * (298\ K)}\right)\right] = .040812\ mol/min$$

$$F_1 \cong F_2$$

$$F_{2,H2O} = x_{H2O} * F_2 = (0.00228) * (.040812\ mol/min) = 9.313 * 10^{-5}\ mol/min$$

To find flux, this flow rate is divided by the membrane's exposed surface area

$$J = \frac{F_{2,H2O}}{A}$$

$$J = \frac{9.313 * 10^{-5}\ mol/min}{1\ cm^2} = 9.313 * 10^{-5}\ \ mol/\min \cdot cm^2$$

$J = Flux\ of\ water\ (L/\min \cdot cm^2)$

$A = Surface\ Area\ (cm^2)$

The permeance was found using the flux and the transmembrane change in water concentration. This change in concentration was found by converting the partial pressure of water to concentration using the ideal gas law, and subtracting from 55.5M, the concentration of water.

$$\boldsymbol{Permeance = \frac{J}{\Delta C}}$$

$\Delta C = Concentration\ Gradient\ (M)$

Appendix D. Permeance Cell Data Tables

The table below shows the raw data collected from the permeance cell tests, as well as the values found through calculations described in Appendix C. These values were used to create the summary shown in Figure 13.

Table 4: Raw Data from Permeance Cell Tests.

Sample: Trial #	Temperature (K)	Relative Humidity %	Partial Pressure Water (Pa)	Flux of Water (mol/min cm^2)	Conc. of Water in Outlet [M]	Permeance of Water (µmol/min cm^2 M)
LV: 1	298.62	7.10	231.22	9.31×10^{-5}	9.31×10^{-7}	1.6780
LV: 2	298.79	7.71	253.63	1.02×10^{-4}	1.02×10^{-6}	1.8396
LV: 3	298.88	5.62	185.87	7.47×10^{-5}	7.47×10^{-7}	1.3477
LV: 4	298.32	9.40	300.71	1.21×10^{-4}	1.21×10^{-6}	2.1845
HV: 1	297.69	10.32	317.95	1.28×10^{-4}	1.28×10^{-6}	2.3146
HV: 2	297.85	13.16	409.34	1.65×10^{-4}	1.65×10^{-6}	2.9783
HV: 3	297.87	12.47	388.35	1.56×10^{-4}	1.56×10^{-6}	2.8254
HV: 4	297.89	10.70	333.62	1.34×10^{-4}	1.34×10^{-6}	2.4272
FC: 1	296.50	11.28	323.53	1.31×10^{-4}	1.31×10^{-6}	2.3646
FC: 2	296.51	11.39	326.88	1.32×10^{-4}	1.32×10^{-6}	2.3891
FC: 3	296.52	8.25	236.91	9.61×10^{-5}	9.61×10^{-7}	1.7315
FC: 4	296.54	7.40	212.76	8.62×10^{-5}	8.62×10^{-7}	1.5549
DH: 1	298.86	16.14	533.16	2.14×10^{-4}	2.14×10^{-6}	3.8662
DH: 2	298.98	11.62	386.59	1.55×10^{-4}	1.55×10^{-6}	2.8022
DH: 3	299.05	7.71	257.58	1.03×10^{-4}	1.03×10^{-6}	1.8666
DH: 4	296.50	10.32	295.99	1.20×10^{-4}	1.20×10^{-6}	2.1634
CF: 1	297.22	9.24	276.76	1.11×10^{-4}	1.11×10^{-6}	2.0180
CF: 2	297.29	9.01	271.01	1.09×10^{-4}	1.09×10^{-6}	1.9756
CF: 3	296.73	6.56	190.78	7.73×10^{-5}	7.73×10^{-7}	1.3933

CF: 4	296.82	8.17	238.90	9.68×10^{-5}	9.68×10^{-7}	1.7442
DI: 1	299.07	8.48	283.64	1.14×10^{-4}	1.14×10^{-6}	2.0553
DI: 2	298.53	9.86	319.39	1.28×10^{-4}	1.28×10^{-6}	2.3186
DI: 3	298.24	10.16	323.47	1.30×10^{-4}	1.30×10^{-6}	2.3505
DI: 4	296.76	8.86	258.14	1.04×10^{-4}	1.04×10^{-6}	1.8851
LN2: 1	298.52	8.63	279.38	1.12×10^{-4}	1.12×10^{-6}	2.0282
LN2: 2	298.66	7.56	246.79	9.93×10^{-5}	9.93×10^{-7}	1.7907
LN2: 3	296.90	11.85	348.17	1.41×10^{-4}	1.41×10^{-6}	2.5414
LN2: 4	296.96	8.78	258.91	1.04×10^{-4}	1.04×10^{-6}	1.8894
DI-CF: 1	298.95	10.55	350.37	1.41×10^{-4}	1.41×10^{-6}	2.5399
DI-CF: 2	299.05	6.56	219.16	8.81×10^{-5}	8.81×10^{-7}	1.5882
DI-CF: 3	299.33	5.18	175.95	7.06×10^{-5}	7.06×10^{-7}	1.2738
DI-CF: 4	299.37	6.10	207.68	8.34×10^{-5}	8.34×10^{-7}	1.5034
LN2-DI: 1	296.90	8.32	244.46	9.90×10^{-5}	9.90×10^{-7}	1.7843
LN2-DI: 2	296.87	9.55	280.06	1.13×10^{-4}	1.13×10^{-6}	2.0446
LN2-DI: 3	296.83	9.01	263.62	1.07×10^{-4}	1.07×10^{-6}	1.9246
LN2-DI: 4	296.80	8.02	234.23	9.49×10^{-5}	9.49×10^{-7}	1.7102
LN2-DI-CF: 1	296.48	8.55	244.93	9.93×10^{-5}	9.93×10^{-7}	1.7903
LN2-DI-CF: 2	296.64	8.78	253.96	1.02×10^{-4}	1.02×10^{-6}	1.8553
LN2-DI-CF: 3	296.60	9.32	268.93	1.09×10^{-4}	1.09×10^{-6}	1.9650
LN2-DI-CF: 4	296.56	9.78	281.52	1.14×10^{-4}	1.14×10^{-6}	2.0573